A Control Methodology to Mitigate the Grid Impact of Wind Turbines

Barry G. Rawn, *Student Member, IEEE*, Peter W. Lehn, *Member, IEEE* , Manfredi Maggiore, *Member, IEEE*

Abstract

This paper introduces a new control topology for converter-interfaced wind turbines. Through a singular perturbation decomposition of the system dynamics, a controller is designed that isolates wind power fluctuations from the power grid. Specifically, the controller causes the closed-loop wind turbine to behave as a simple first order power filter, where power injected into the grid is a low pass filtered version of the incident wind power. It is shown that a turbine hub-speed instability imposes a limit on the largest filtering time constant that may be safely implemented. A linearized analysis is used to calculate how small a filter time constant can be implemented to obtain regulation of the tip-speed ratio for the widest range of frequencies. The methodology thus offers the possibility to either deliver a filtered power at sub-optimal conversion efficiency, or to track peak wind power. It is mathematically demonstrated that the control structure achieves the regulation of torsional dynamics and the dc-link capacitor voltage without involving the grid-side converter controls, thus eliminating the influence of those dynamics on the grid. Simulation studies are used to demonstrate the methodology's viability, and explore the associated trade-offs.

Index Terms

wind power generation, energy storage, dynamics, power generation control

I. INTRODUCTION

In many areas of the world, significant contributions by wind energy conversion systems to the generation mix are planned. Compliance with new grid codes [1] and contribution to system regulation by wind farms [2], [3] are being studied. It has been commented that the sacrifice of energy capture in order to obtain better control of wind farm power output may become more common [4], [1]. However, in most installations and published research, the power delivered to the grid is a consequence of the primary goals of tip-speed regulation, shaft damping, and dc-link capacitor voltage regulation. Grid power is therefore a *system output* that can contain fast variations caused by the excitation of conversion system modes by wind turbulence. This complicates studies of grid impact.

This paper presents a control structure for a system with a fully-rated converter, where the power delivered to the grid is defined as a *control input* P_{ref}. An analytical separation into fast and slow time scale models is central to the approach. It is first shown that the variations of the shaft, generator speed and capacitor voltage constitute a fast subsystem that can be regulated without exchanging energy with the grid. The stability implications of imposing a desired power extraction P_{ref} on the more slowly evolving turbine hub are then examined.

The control structure is used to implement a methodology where P_{ref} is based on windpseed to deliver a filtered version of available power. The slow time scale model is analyzed in conjunction with wind models to gain insight into the bounds on the implementable time constant. The concept of employing turbine kinetic energy to absorb fluctuations and deliver a de-rated, filtered power has also been studied in [5],[6]. In these approaches, as well as in the one proposed here, a trade-off of filtered power for decreased energy capture and increased speed variations must be accepted. Simulation results quantify this trade-off and demonstrate the isolating properties of the control structure.

II. MODELING AND SYSTEM STRUCTURE

A useful model must include the characteristic frequency content of wind speeds, the static curve that describes the aerodynamic conversion of energy by the bladed turbine rotor, and a dominant mechanical mode between the inertia of the rotor and the generator mass. In this work, a wind turbine with parameter values as in [7], interfaced through a back-to-back converter system, has been studied.

A. Wind Modeling

Over periods shorter than an hour, wind speed can be approximated as the superposition of a slowly varying mean speed $\overline{v}_w$ and N sinusoidal components having amplitudes A_i and random phases ψ_i.

$$v_w(t) = \overline{v}_w + \sum_{i=0}^{N} A_i cos(\omega_i t + \psi_i) \tag{1}$$
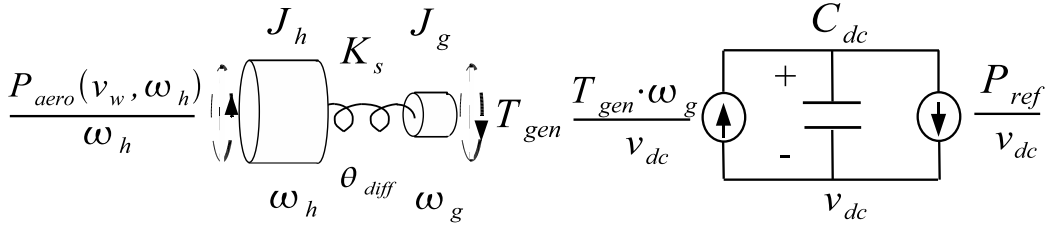
Fig. 1. Schematic representation of system model showing parameters and states.

The frequencies ω_i and amplitudes A_i of these N components are given by an empirically determined spectral density function. For this work, the von Karman distribution [8] is used.

$$S_{vv}(\omega_i) = \frac{0.475\sigma^2 \frac{L}{\overline{v}_w}}{\left[1 + \left(\frac{\omega_i L}{\overline{v}_w}\right)^2\right]^{\frac{5}{6}}} \tag{2}$$

The distribution (2) depends on the mean speed $\overline{v}_w$, the roughness of the surrounding landscape (as described by a characteristic length scale L), and the standard deviation σ of wind speeds. The frequencies ω_i are chosen to be logarithmically spaced in order to properly represent the frequency content of (2). The amplitude A_i of each discrete frequency component is chosen to give it a power equal to that contained in a certain frequency band, which is found by calculating the area under the density function $S_{vv}(\omega_i)$. The amplitude is given as follows:

$$A_i(\omega_i) = \sqrt{2 \cdot \frac{[S_{vv}(\omega_i) + S_{vv}(\omega_{i+1})][\omega_{i+1} - \omega_i]}{2}}. \tag{3}$$

B. Conversion System Modeling

The power coefficient, C_P, describes the efficiency with which wind energy is extracted by the turbine blades. C_P depends on the tip-speed ratio, λ, defined as

$$\lambda = \frac{R\omega_h}{v_w} \tag{4}$$

where ω_h is the rotational speed of the rotor, v_w is the wind speed, and R is the radius of the rotor. C_p (shown in Fig. 2) determines the aerodynamic power, P_{aero}, extracted from the available wind power:

$$P_{aero} = \frac{1}{2}\rho\pi R^2 C_p(\lambda) v_w^3. \tag{5}$$

The shape of the C_P curve causes maxima in both the speed-power and speed-torque curves. Maximum power is obtained when $\lambda = \lambda^{opt}$ as shown in Fig. 2.
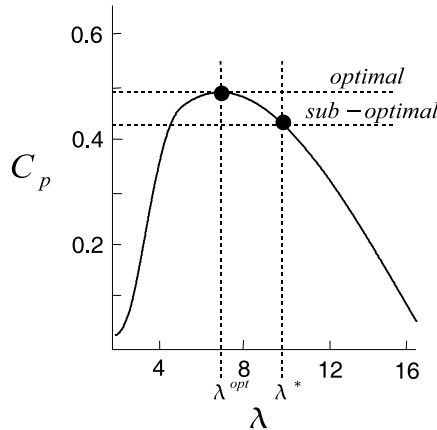

Fig. 2. C_p curve. Sub-optimal efficiency occurs for $\lambda^* > \lambda^{opt}$.

This aerodynamic relation determines the dynamics of the turbine rotor speed ω_h and depends on the dimensionless ratio λ, rather than the wind speed or rotor speed individually. Operation can occur at a sub-optimal conversion efficiency around a tip-speed ratio $\lambda^* > \lambda^{opt}$.

The mechanical components of a wind turbine system are commonly simplified to a two-mass model with a flexible coupling having stiffness K_s [9],[10]. In the implementation chosen for this work, these elements are cascaded through an AC-DC-AC converter as represented in Fig 1. Through the application of vector controls for the machine-side converter currents, the electromagnetic torque and flux inside the generator can be controlled with a high bandwidth [11]. Therefore, it is assumed that the torque T_{gen} established in the generator is a control input. The flux is simply set constant at Φ_{rated}. The active and reactive power leaving the grid-side converter can also be regulated using high bandwidth vector controls. The active power is chosen as an independent control input P_{ref}, and reactive power Q_{ref} can be specified as desired. The converter is thus simplified to a differential equation for the dc-link capacitor voltage, where the contol inputs T_{gen} and P_{ref} enter as dictated by power balance.

The uncontrolled state-space system associated with Fig. 1 is as follows:

$$
\begin{aligned}
\frac{d\omega_h}{dt} &= \frac{1}{J_h}\left(P_{aero}(v_w(t),\omega_h)/\omega_h - K_s\theta_{diff}\right) \\
\frac{d\theta_{diff}}{dt} &= \omega_h - \omega_g \\
\frac{d\omega_g}{dt} &= \frac{1}{J_g}\left(K_s\theta_{diff} - T_{gen}\right) \\
\frac{dv_{dc}}{dt} &= \frac{T_{gen}\omega_g - P_{ref}}{C_{dc}v_{dc}}
\end{aligned}
\tag{6}
$$

where T_{gen} and P_{ref} are control inputs, $v_w(t)$ is a time-varying wind speed input signal, and other symbols are defined as in Fig. 1.

C. System Analysis

Because of the large value of J_h, the equations (6) have a singularly perturbed form indicating that their dynamics take place on two distinct time scales. For analysis and control design, the system (6) can be formally separated into two independent subsystems of equations.

The separation proceeds by assuming that the faster states of the system are stable and settle to steady-state values. This simplifies the influence of the fast states on the slow state. The control input T_{gen} is defined as having a slow component $\overline{T}_{gen}$, and a fast component $\widetilde{T}_{gen}$ that is zero at steady-state

$$
T_{gen} = \overline{T}_{gen} + \widetilde{T}_{gen}.
\tag{7}
$$

By setting the left hand side of the last three equations of (6) to zero, quasi-steady state values for θ_{diff}, ω_g and the 'slow' control input $\overline{T}_{gen}$ can be found

$$
\begin{aligned}
\theta_{diff} &= \overline{T}_{gen}/K_s \\
\omega_g &= \omega_h \\
\overline{T}_{gen} &= P_{ref}/\omega_g.
\end{aligned}
\tag{8}
$$

The above conditions correspond to a lack of torsional oscillations, and power balance across the converter. The quasi-steady state dc voltage $\overline{v}_{dc}$ is unspecified by (8) and can be freely assigned. The quasi-steady state values, which vary on a slow time scale, are substituted in the first equation of (6) to obtain a slow subsystem with a single state $\overline{\omega}_h$, time-varying input $v_w(t)$, and control input P_{ref}

$$
\frac{d\overline{\omega}_h}{dt} = \frac{P_{aero}(v_w(t),\overline{\omega}_h) - P_{ref}}{J_h\overline{\omega}_h}.
\tag{9}
$$

The fast dynamics of (6) are viewed as evolving on their own time scale $\tau = J_h t$. On this time scale, it is assumed that the state ω_h changes so slowly that it can be replaced with a constant ξ_0. Defining

$$
\begin{bmatrix} y_1 \\ y_2 \\ y_3 \end{bmatrix} = \begin{bmatrix} \theta_{diff} - \frac{1}{K_S}\frac{P_{ref}}{\omega_g} \\ \omega_g - \omega_h \\ v_{dc} - \overline{v}_{dc} \end{bmatrix},
\tag{10}
$$

the substitution

$$
T_{gen} = P_{ref}/\omega_g + \widetilde{T}_{gen}
\tag{11}
$$

into the last three equations of (6) yields the dynamic equations of the fast subsystem

$$
\begin{aligned}
\frac{dy_1}{d\tau} &= -y_2 \\
\frac{dy_2}{d\tau} &= \frac{1}{J_g}\left(K_s y_1 - \widetilde{T}_{gen}\right) \\
\frac{dy_3}{d\tau} &= \frac{\xi_0 + y_2}{C_{dc}(\overline{v}_{dc} + y_3)}\widetilde{T}_{gen}.
\end{aligned}
\tag{12}
$$

The control input in (12) is $\widetilde{T}_{gen}$. Equations (12) may be used exclusively for the study of fast dynamics, while (9) is used for the study of slow dynamics, which may be interpreted as the motion of the system's centre of inertia.
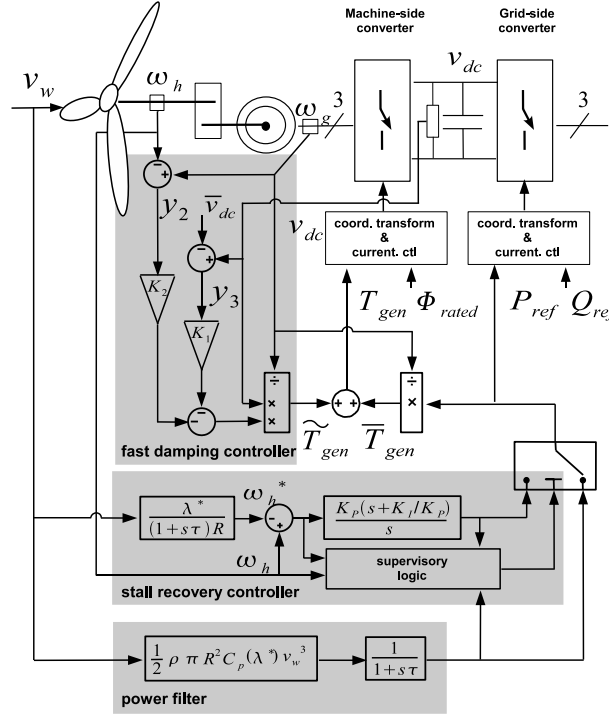
Fig. 3. Full-converter interfaced wind turbine with control structure.

III. CONTROL METHODOLOGY

A. Control Input T_{gen}

The two components of the control input T_{gen} are constructed as shown in Fig 3. Setting $\overline{T}_{gen}$ according to (8) achieves an average power balance across the back-to-back converter. The component $\widetilde{T}_{gen}$ is designed to damp torsional and capacitor voltage oscillations contained in the fast subsystem (12). While (12) is nonlinear, it is only weakly so. This becomes evident from substituting the control law of Fig. 3

$$\widetilde{T}_{gen} = \frac{\overline{v_{dc}} + y_3}{\xi_0 + y_2} \left(-K_1 y_3 - K_2 y_2\right) \tag{13}$$

where K_1 and K_2 are positive gains. From the approximation $\xi_0 + y_2 \approx \xi_0$ and algebraic manipulation, one obtains:

$$\begin{bmatrix} \frac{y_1}{d\tau} \\ \frac{y_2}{d\tau} \\ \frac{y_3}{d\tau} \end{bmatrix} = \begin{bmatrix} 0 & -1 & 0 \\ \frac{K_s}{J_g} & \frac{1}{J_g}\frac{\overline{v_{dc}}}{\xi_0}K_2 & \frac{1}{J_g}\frac{\overline{v_{dc}}}{\xi_0}K_1 \\ 0 & -\frac{1}{C_{dc}}K_2 & -\frac{1}{C_{dc}}K_1 \end{bmatrix} \begin{bmatrix} y_1 \\ y_2 \\ y_3 \end{bmatrix} +$$
$$\begin{bmatrix} 0 \\ +\frac{1}{J_g\xi_0}K_2 y_3 y_2 & +\frac{1}{J_g\xi_0}K_1 y_3^2 \\ -\frac{1}{C_{dc}\xi_0}K_2 y_2^2 & -\frac{1}{C_{dc}\xi_0}K_1 y_3 y_2 \end{bmatrix} \tag{14}$$

which has the form of a linear system $\dot{x} = Ax$ with a perturbation $g(x)$

$$\dot{x} = Ax + g(x) \tag{15}$$

that vanishes at the origin of the transformed system, which in this case corresponds to the quasi-steady state values of θ_{diff}, ω_g, and v_{dc}. The perturbation $g(x)$ has a higher order, so it does not affect the linearization. Hence, if the linear part of the system is stable through appropriate choice of K_1 and K_2, then the origin of the boundary system is locally exponentially stable [12].

Influence of the torsional dynamics and dc-link dynamics on the grid through delivered active power is eliminated by using the generator torque T_{gen} to achieve damping. The energy required to regulate these variations is exchanged with the turbine hub rather than the grid. No inter-turbine or turbine-grid modes can ever exist in the proposed controller.

B. Control Input P_{ref}

The control input P_{ref} and external input P_{aero} influence the speed $\overline{\omega}_h$ of the turbine hub's centre of inertia according to (9). These slow dynamics are common to all converter interfaced wind turbines.

P_{ref} could be chosen arbitrarily, provided it does not exceed the available power for too long. Ideally, it is desired to demand a filtered power [5],[6] or one based on grid variables [2],[3],[13]. The torque-speed curves associated with such goals must be examined carefully, because they introduce the possibility of instability. A power command P_{ref} that changes more slowly than turbine hub speed will produce a generator torque approaching that of a constant power characteristic as in Fig 4.

Fig. 4 plots the aerodynamic torque and generator torque for the case of constant wind speed, and a constant power P_{ref} that is less than the maximum available wind power. An equilibrium is reached at the speed $\overline{\omega}_h{}^s$, where exactly P_{ref} is being extracted from the wind. For a range of lower speeds, more than P_{ref} is available from the wind, causing an accelerating torque that drives the hub speed back toward $\overline{\omega}_h{}^s$. Variations of the wind can change the size of this region of restoring torque, and even eliminate it. Maintaining a constant P_{ref} in the presence of such variations may cause instability. De-rating P_{ref} to be less than the available power increases the domain of stability of the turbine hub. This can be illustrated by studying a simple example.

Choose a constant power P_{ref} based on a mean wind speed $\overline{v}_w$, as follows:

$$P_{ref} = \frac{1}{2}\rho\pi R^2 C_p(\lambda^*)\overline{v}_w^3 \tag{16}$$

$$\lambda^* \geq \lambda^{opt}, C_p(\lambda^*) \leq C_p(\lambda^{opt}). \tag{17}$$

Choosing $\lambda^* = \lambda^{opt}$ extracts a maximum power, while a higher λ^* extracts a de-rated power.

Now, let the wind have a simple periodic variation around $\overline{v}_w$, with a period T, as in Fig. 5(a). The two aerodynamic torque characteristics corresponding to $v_{w_{max}}$ and $v_{w_{min}}$ in the speed-torque plane are shown in Fig. 5(b). The generator torque given by $P_{ref}/\overline{\omega}_h$ is also plotted. From the upper curve, we identify a critical speed $\overline{\omega}_h{}^u$. No accelerating torque exists below this speed for any portion of the period T. Therefore, if $\overline{\omega}_h$ drops below this speed, it will collapse toward zero.

The trajectory of the operating point is shown in Fig 5(b) for the case where the maximum power available at windspeed $\overline{v}_w$ is demanded by choosing $\lambda^* = \lambda_{opt}$. The period T is short enough that the turbine never settles at a constant speed. No region of accelerating torque exists during the interval of low wind speed. However, the wind speed increases before $\overline{\omega}_h$ drops below $\overline{\omega}_h{}^u$, and therefore the given wind input provokes a stable cycle for the chosen constant power.

In Fig. 5(c), the period and amplitude of the wind input have been increased. The response of the turbine is shown for a power based on $\lambda^* > \lambda_{opt}$ (dashed) is shown in addition to that based on $\lambda = \lambda^{opt}$ (solid). In each case the excursion of the turbine hub speed is larger because a larger energy variation must now be absorbed. In the case of the power based on λ^{opt} (solid line), the wind variation causes a period of hub deceleration long enough that the hub speed dips below $\overline{\omega}_h{}^u$. Hence a collapse of the hub speed is unavoidable. The trajectory associated with the power level based on $\lambda^* > \lambda^{opt}$(dashed line) remains stable.

IV. APPLICATION TO POWER FILTERING

It is clear that stability will limit the duration and size of an arbitrary power demand. Over long periods of time, the power demanded must be chosen to follow the slow variations of the wind resource. The example of Section III B. can be viewed as an approximation of the situation where changes in the mean wind speed are being tracked, but faster fluctuations must
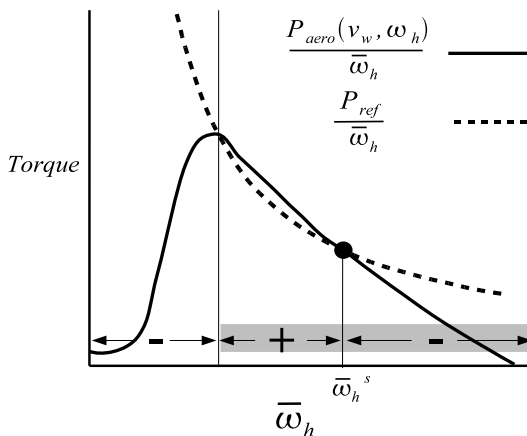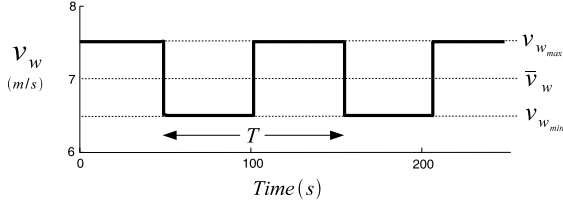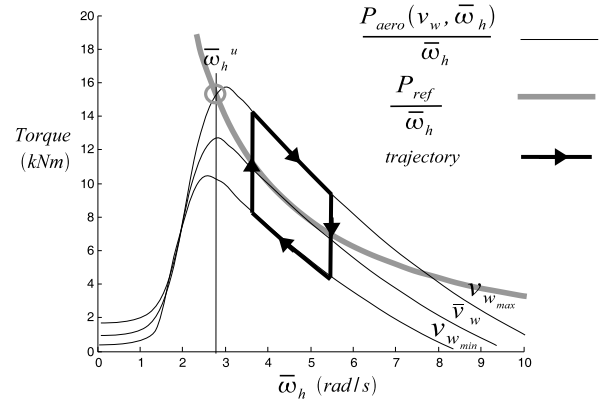

Fig. 4. Torque-speed characteristic for constant power extraction. Sign of net torque (+ accelerating, - decelerating) is marked. A stable interval (shaded) of restoring torque exists for the operating point $\overline{\omega}_h{}^s$.

(a) A simple periodic wind speed input varying between $v_{w_{max}}$ and $v_{w_{min}}$ with period T. $\overline{v}_w = 7m/s$, $T = 105s$.

(b) Response of turbine hub to wind input for constant power extraction.
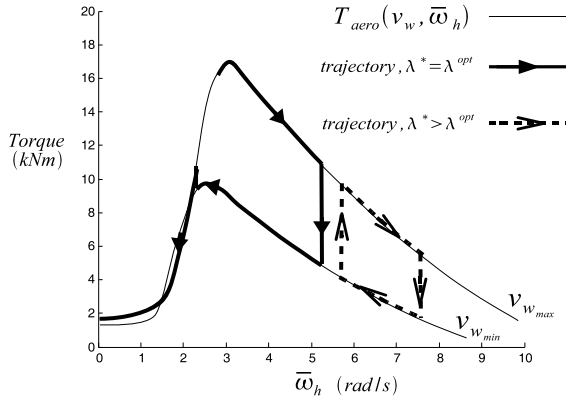
(c) Response to slower, larger wind variation for optimal power (solid) and de-rated power (dashed) cases.

Fig. 5. Dynamics of constant power extraction for square wave periodic wind input. Extraction of maximum (solid) and de-rated (dashed) power levels based on mean wind speed $\overline{v}_w$ is considered. A larger, slower wind variation provokes a collapse of hub speed when too high an average power level is demanded.

be absorbed. The stored kinetic energy of the turbine hub can be employed to further contain fluctuations in available wind power, in addition to absorbing torsional fluctuations. It has been demonstrated that considerable smoothing of output power can be obtained by de-rating the demanded power [5]. In this section the bounds placed on safe operation as a power filter are demonstrated by simulation, and explained through analysis of the models of Section I. Guidelines for the design of the power filter time constant and de-rating are obtained, and performance is reported in Section V.

The output power P_{ref} is chosen to be based on a wind speed measurement and an adjustable de-rating $C_p(\lambda^*)$, filtered with a time constant τ :

$$\dot{P}_{ref} = \frac{1}{\tau} \left(\frac{1}{2} \rho \pi R^2 C_p(\lambda^*) v_w^3 - P_{ref} \right) \tag{18}$$

$$\lambda^* \geq \lambda^{opt}, C_p(\lambda^*) \leq C_p(\lambda^{opt}).$$

It is necessary to provide a control structure that guarantees stable operation in all conditions. If instability does occur, it is detected by the supervisory logic block in the *stall recovery controller* shown in Fig. 3, and P_{ref} is specified by a speed regulator instead of the power filter. P_{ref} then varies to stabilize a reference turbine hub speed ω_h^*, which is a low-pass filtered version of $\frac{\lambda^*}{R} v_w(t)$. When the power level specified by the speed regulator enters a suitable neighbourhood of the level being specified by the power filter, the supervisory control reverts P_{ref} to the power filter signal from (18).

Robust detection of instability can be based on the simultaneous satisfaction of several conditions related to the operating point and its dynamics:

- decreasing turbine hub speed
- decrease of $\lambda(t)$ below a threshold
- increase of the derivative $\partial \overline{T}_{gen}/\partial \overline{\omega}_h$ above a threshold.

The speed regulator is the following simple proportional-integral feedback controller

$$P_{ref} = K_P(\overline{\omega}_h - \overline{\omega}_h^*) + K_I \eta$$
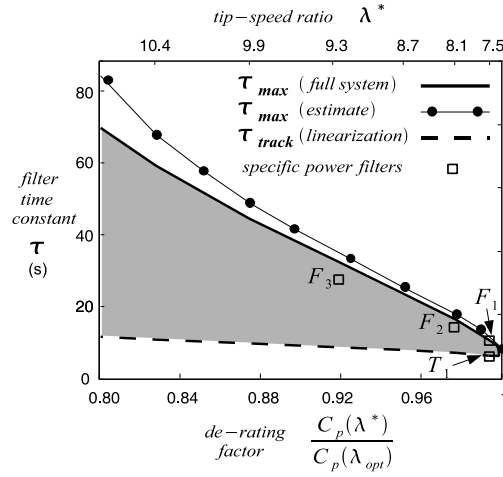$$\dot{\eta} = \overline{\omega}_h - \overline{\omega}_h^* \tag{19}$$

Fig. 6. Operating envelope of power filter. Maximum filter time constant τ_{max} (solid) and minimum filter time constant τ_{track} (dashed) for a given de-rating and corresponding tip-speed ratio λ^* are shown. Certain filters F_3-F_1 and T_1 are selected to demonstrate performance in Section V.

where $\overline{\omega}_h{}^*$ is determined by the filtered wind speed and λ^* as shown in Fig. 3. At the instant t_0 when a switch of control is made, the continuity of P_{ref} (i.e. $P_{ref}(t_0{}^+) = P_{ref}(t_0{}^-)$) is assured by initializing the integral state η appropriately.

A. Stability Threshold

The response of the full nonlinear system (6) to a 70 minute time series of measured wind speed was simulated over a wide range of parameters λ^* and τ. For each pair, state variables were monitored for instability. A maximum tolerable time constant τ_{max} was defined as the largest τ for which no interventions by the supervisory control occurred. Fig. 6 shows the dependence of τ_{max} on the de-rating of P_{ref}. The stability threshold places an upper bound on the operating envelope of the system. A rough estimate of the threshold (also shown in Fig 6) can be produced using a simpler method based on a single representative sinusoidal windspeed and the slow subsystem (9). The approximations that yield this estimate provide some insight into the system, but must be used with caution. The method is derived from the study of a linearization of (9), which gives further guidance on the selection of τ and λ^*.

B. Filter Design from Linearization

A linearized model of the speed $\overline{\omega}_h$ is obtained by substituting (18) in (9), linearizing at a stable operating point $v_w{}^{op} = \overline{v}_w$, $P_{ref} = 1/2\rho\pi R^2 C_p(\lambda^*)\overline{v}_w{}^3$, $\overline{\omega}_h{}^{op} = \frac{\lambda^*}{R}\overline{v}_w$, and taking Laplace transforms. This yields a single-input, single-output transfer function $G(s)$ from the wind speed to the turbine hub speed:

$$\Delta\overline{\omega}_h = G(s)\Delta v_w$$

$$= \frac{\lambda^*}{R} \cdot \frac{\left(1 + \frac{s}{\omega_{zero}}\right)}{\left(1 + \frac{s}{\omega_{pole}}\right)\left(1 + \frac{s}{\omega_{filt}}\right)}\Delta v_w \tag{20}$$

where

$$\omega_{filt} = \frac{1}{\tau} \tag{21}$$

$$\omega_{zero} = \omega_{filt} \frac{1}{1 + \frac{3 \cdot C_p(\lambda^*)}{\left(-\left.\frac{dC_p}{d\lambda}\right|_{\lambda^*}\right) \cdot \lambda^*}} \tag{22}$$

$$\omega_{pole} = \frac{\rho\pi R^3}{2J_h} \cdot \frac{v_w{}^{op2}}{\overline{\omega}_h{}^{op}}\left(-\left.\frac{dC_p}{d\lambda}\right|_{\lambda^*}\right) \tag{23}$$

The dc gain of the Bode plots shown in Fig. 7 is determined by the desired tip-speed ratio λ^*. Perfect regulation of the desired tip-speed ratio (i.e. power tracking) would result in a Bode plot with gain λ^*/R and a phase of $0°$ at all frequencies. The power filter introduces the left-half plane zero and pole ω_{zero} and ω_{filt}, which have important effects on the response of the turbine hub speed. For small τ, the power filter has little effect and the time constant ω_{pole} of the turbine hub dominates the response, as shown by the gray line in Fig. 7.
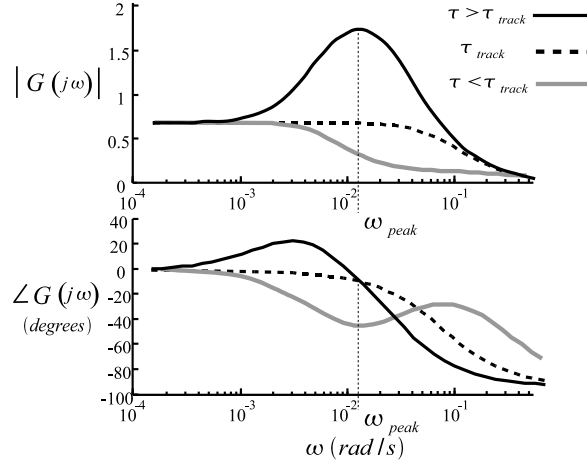
Fig. 7. Bode plots of the transfer function $G(j\omega)$ for different filter time constants τ. For $\tau = \tau_{track}$ the closest possible tracking of λ^* occurs. For $\tau > \tau_{track}$, filtering and large λ variations occur due to a resonant peak at ω_{peak}.

For a unique filter time constant, τ_{track}, the natural response of the turbine hub is compensated by ω_{zero}, generating a first order response that maintains the gain close to its DC-value up to $1/\tau$. This value of τ produces tracking for the largest range of frequencies possible; it can be immediately obtained from the relations (22) and (23).

As τ increases beyond τ_{track} (solid dark line of Fig. 7), the model develops a resonant peak at a frequency ω_{peak}. The phase-leading response has the physical explanation that the hub speed response to wind variations is larger than that necessary to maintain the tip-speed ratio λ^*, and that absorption of wind fluctuations is occurring.

The linear system (20) can not capture the instability that gives rise to the threshold time constant τ_{max}, but it provides the resonant frequency ω_{peak} of a given operating point. To produce an estimate of τ_{max}, it is assumed that the crucial response of the speed $\overline{\omega}_h$ occurs at this frequency. The wind speed input is therefore simplified to a mean speed and a single sinusoidal component

$$v_w(t) = \overline{v}_w + V_w cos\left(\omega_{peak}t\right). \tag{24}$$

This representative sinusoidal signal should have the same power as the frequency components of the wind that may affect stability by causing deviations in tip-speed ratio. The resonant hump of (20) shows the frequency range of concern, and the power spectral density (2) describes the power in a given range. Therefore, the amplitude V_w is based on the area under (2) at frequencies greater than the beginning of the resonant hump of (20):

$$V_w \approx \sqrt{2 \int_{\omega_{zero}/2}^{\infty} S_{vv}(\omega_i)d\omega} \tag{25}$$

where the integral is discretely approximated.

When the slow subsystem (9) with control input (18) and wind input (24) is simulated for a set of initial conditions, the turbine hub speed either collapses or settles to a limit cycle for each one. Further study of this simplified nonlinear system could produce an analytical result on how the existence of a stable limit cycle depends on the parameter τ. Iterative simulations were used to construct the estimate of τ_{max} shown in Fig. 6.

For each conversion efficiency $\lambda^* \geq \lambda^{opt}$, the filter time constants τ_{track} and τ_{max} define an operating envelope for the conversion system that ranges between tracking of λ^* and the absorption of wind power fluctuations. The operating envelope is the shaded region in Fig. 6. Any trade-off between maximizing energy capture ($\lambda^{opt}, \tau_{track}$) and delivering smooth power ($\lambda^* > \lambda^{opt}, \tau_{max}$) can easily be selected. Several pairs of parameters (marked as F_3, F_2, F_1, and T_1) have been selected as examples of possible filters to be evaluated in Section V.

V. RESULTS

Measured wind time series were obtained from the same test site as used in [14] through a communication with the authors, and employed in all simulations.

A. Adjustable Power Filter Performance

Fig. 8 shows the delivered power and turbine hub speed over 10 minutes for power tracking mode at high efficiency (T_1 on Fig. 6) and for power filtering mode at de-rated efficiency (F_3). The maximum available power P_{max} is also plotted. The
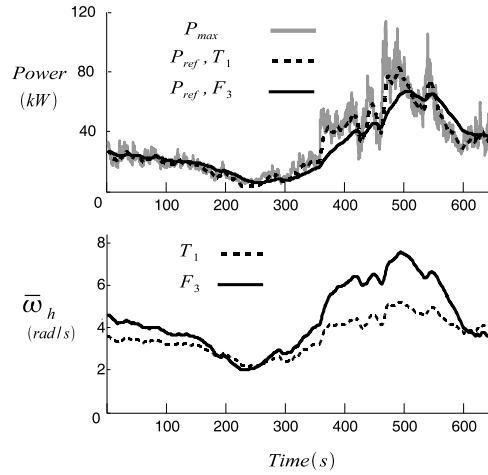
Fig. 8. Power filtering (F_3) and power tracking (T_1) modes, compared against available wind power P_{max}. Speed variations are broader for the parameter pair F_3, and a smoother power is delivered.

delivered power clearly tracks P_{max} more closely for the filter T_1. However, the delivered power obtained with the filter F_3 is smoother, though it must be less on average due to its de-rating. It is evident from the plot of turbine hub speed that this smoothing is possible due to large variations around a higher average speed than of the filter T_1. A more quantitative demonstration of the trade-offs of power filtering mode is provided by the results of several 50 minute simulations summarized in Table I. The amount of energy captured relative to the maximum available is shown, as are the filter time constant τ, average speed, and standard deviation of speeds. Operation in filtering mode reduces capture, and higher average speed and larger speed variations are evident from the last two columns. For operation at larger de-ratings, practical machine speed limits would likely be reached before the filtering time-constant τ reached the maximum imposed by the aerodynamic stability limit.

TABLE I
SUMMARY: ENERGY CAPTURE AND SPEED VARIATIONS IN FILTERING MODE

|	Energy Capture(%)	τ (s)	Average Hub Speed (rad/s)	Std. Dev (rad/s)
T_1	99.4	6	3.72	0.42
F_1	99.3	11	3.69	0.65
F_2	97.6	16	3.99	0.80
F_3	91.5	28	4.57	1.01

B. Containment of Power Variations

Choosing a filtered power P_{ref} attenuates the wind power variations delivered to the grid. As discussed, the filter time constant must be set within the ability of the turbine hub inertia to absorb fluctuations. Fig 9 shows the frequency content of delivered power for the optimal power tracking parameters T_1, and the de-rated power filtering parameters F_3.

Specifying P_{ref} based on wind speed rather than states of the fast subsystem completely removes the influence of those states from the delivered power. Fig. 9(b) compares the generator power with the power P_{ref} delivered to the grid. A hump in the frequency content of the generator power around 2 Hz corresponds to the torsional resonance [15],[16]. The control structure prevents this torsional resonance from being coupled to power system variables. Variations of the dc-link capacitor voltage and mechanical system states occur due to continual forcing of the torsional resonance by wind disturbances. The effect of the control law defined for $\widetilde{T}_{gen}$ on these states is demonstrated in Fig. 10. Variations in the states are well contained.

VI. CONCLUSIONS

As a step toward understanding the limits of imposing a desired power output on wind turbines, a new control structure has been introduced that can cause them to appear as adjustable power filters. It has been shown how this allows a range of operation modes (from power tracking to power filtering) over a range of conversion efficiencies. However, a stability limit on the filter time constant used in power filtering is demonstrated. It was also shown that it is possible to regulate torsional and dc-link voltage dynamics using only the machine-side converter controls, eliminating the influence of internal modes on the grid.
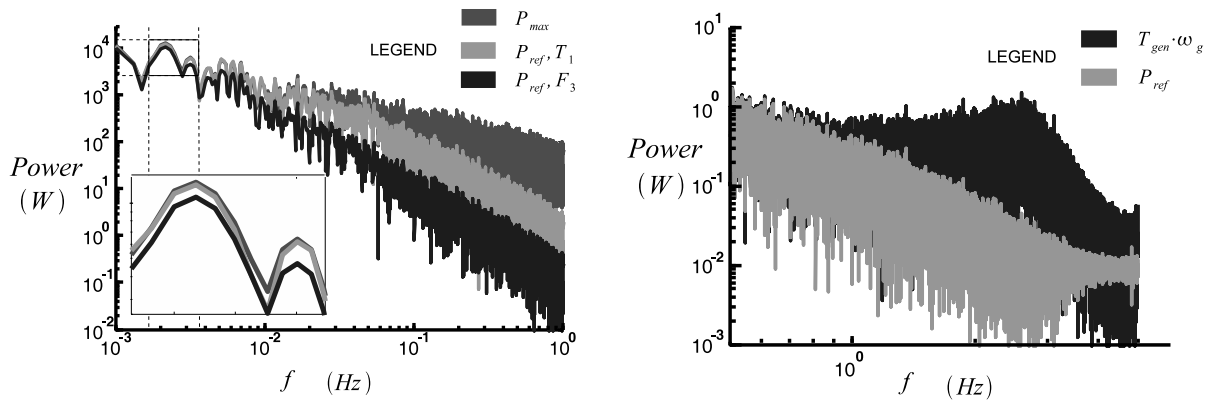
(a) Maximum available wind power and range of possible filtered powers.

(b) Containment of power fluctuations within conversion system

Fig. 9. Frequency content of power flows. In Fig. 9(a), filters F_3 and T_1 demonstrate power filtering and maximum power tracking in the frequency domain. Inset shows reduced capture at low frequency for F_3 due to de-rating. In Fig 9(b), delivered power P_{ref} is compared with the generator power. Power variations due to torsional resonance are isolated.

In today's wind installations, providing a filtered power may not yield a monetary value that can compensate the economic losses associated with decreased energy capture. However, in the future, problems arising from increased wind power penetration may drive a need to exploit all the potential operating modes of installed wind turbine generators. For example, a strategy of shifting between optimal power tracking and a filtered power extraction mode by adjusting the filter time constant τ and tip-speed ratio λ^* may become attractive. A control structure where delivered power is a control input is a natural arrangement for implementing new control functions for wind turbines, and for studying their impact. Given the growing interest in allowing wind farms to contribute to the regulation of power systems, the methodology and analyses of fundamental limitations presented here warrant further investigation.

REFERENCES

[1] B. Rabelo and W. Hofmann, "Wind generator control in compliance with new norms," presented at the IEEE International Symposium on Industrial Electronics, June 9–11 2003.

[2] F. Hughes, O. Anaya-Lara, N. Jenkins, and G. Strbac, "Control of DFIG-based wind generation for power network support," *IEEE Transactions on Power Systems*, vol. 20, no. 4, pp. 1958–1966, 2005.

[3] F. Koch, I. Erlich, F. Shewarega, and U. Bachmann, "Dynamic interaction of large offshore wind farms with the electric power system," presented at the IEEE Bologna PowerTech Conference, Bologna, Italy, June 23–26, 2003.

[4] T. Gjengedal, "Large scale wind power farms as power plants," *Wind Energy*, vol. 8, no. 3, pp. 361–373, 2005.

[5] L.Ran, J. Bumby, and P. Tavner, "Use of turbine inertia for power smoothing of wind turbines with a DFIG," in *11th International Conference on Harmonics and Quality of Power*, Sept.12–15 2004, pp. 106–111.

[6] C. Sourkounis and B. Ni, "Optimal control structure to reduce the cumulative load in the drive train of wind energy converters," presented at the 11th European Conference on Power Electronics and Applications, Dresden, Germany, Sept. 11–14 2005.

[7] T. Petru, "Modelling of wind turbines for power systems studies," Ph.D. dissertation, Chalmers University of Technology, Göteborg,Sweden, June 2003. [Online]. Available: http://www.elkraft.chalmers.se/Publikationer/EMKE.publ/Abstracts/2003/tomasPhD.html

[8] C. Nichita, D. Luca, B. Dakyo, and E. Ceanga, "Large band simulation of the wind speed for real time wind turbine simulators," *IEEE Transactions on Energy Conversion*, vol. 17, no. 4, pp. 523–529, December 2002.

[9] V. Akhmatov, H. Knudsen, and A. Nielsen, "Advanced simulation of windmills in the electric power supply," *Electrical Power & Energy Systems*, vol. 22, pp. 421–434, 2000.

[10] B. C. W.E. Leithead, "Control of variable speed wind turbines: design task," *International Journal of Control*, vol. 73, no. 13, pp. 1189–1212, 2000.

[11] R. Pena, R. Cardenas, R. Blasco, G. Asher, and J. Clare, "A cage induction generator using back-to-back PWM converters for variable speed grid connected wind energy system," in *IECON'01: The 27th Annual Conference of the IEEE Industrial Electronics Society*, 2001, pp. 1376–1381.

[12] H. Khalil, *Nonlinear Systems*. Prentice-Hall, 2002.

[13] T. Gjengedal, "Integration of wind power and the impact on power system operation," presented at the Large Engineering Systems Conference on Power Engineering, May 7–9 2003.

[14] T. Thiringer and J. Dahlberg, "Periodic pulsations from a three-bladed wind turbine," *IEEE Transactions on Energy Conversion*, vol. 16, no. 2, pp. 128–133, June 2001.

[15] T. Thiringer, T. Petru, and C. Liljegren, "Power quality impact of a sea located hybrid wind park," *IEEE Transactions on Energy Conversion*, vol. 16, no. 2, pp. 123–127, June 2001.

[16] A. Hansen, P. Sorensen, L. Janosi, and J. Bech, "Wind farm modeling for power quality," *The 27th Annual Conference of the IEEE Industrial Electronics Society*, pp. 1959–1964, 2001.
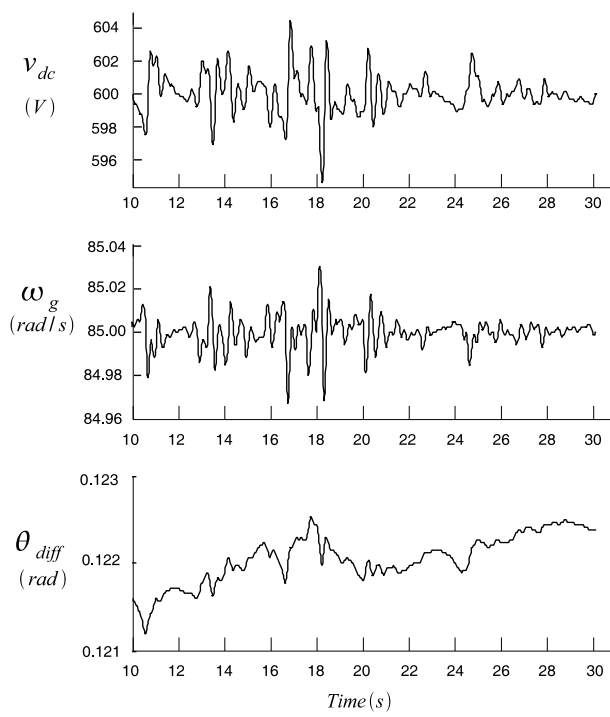
Fig. 10.   Regulation of capacitor and torsional oscillations.